3D Geometric Assessment of a Commercial RTK/PPP Visual Positioning Mobile Sensor

Maria Valasia Peppa [1], Luca Morelli [2], Fabio Remondino [2], Jon P. Mills [1]

[1] School of Engineering, Newcastle University, Newcastle upon Tyne, NE1 7RU, United Kingdom
Email: (maria-valasia.peppa, jon.mills)@newcastle.ac.uk

[2] 3D Optical Metrology (3DOM) unit, Bruno Kessler Foundation (FBK), Trento, Italy
Email: (lmorelli, remondino)@fbk.eu

Technical Commission II

Keywords: 3D reconstruction, direct georeferencing, photogrammetry, point cloud, PPP, RTK, sensor orientation, SLAM

ABSTRACT

The Leica GS18i visual positioning system, introduced in 2021, uses 3D imaging to measure points beyond the reach of conventional GNSS receivers, such as building façades. By leveraging RTK and PPP GNSS capabilities, it enables continuous image acquisition during surveys. This study assessed its 3D geometric accuracy in both open and complex environments with poor GNSS signals. Two field tests at Vindolanda Roman Fort and Newcastle University's Quadrangle Gateway served to evaluate processing results within the proprietary Leica Infinity and Agisoft Metashape. Results demonstrated 3D RMSEs of ca 3.5 cm in RTK mode without GCPs and 2.5 cm when all images are triangulated with a single GCP. The system achieved consistent cm-level accuracy and precision under challenging conditions with sufficient initial GNSS RTK image orientation. Comparative analyses with Canon DSLR datasets highlighted the GS18i system's efficiency, though software differences emerged.

1. INTRODUCTION

An important advancement in mobile and dynamic geospatial data acquisition is eliminating the reliance on ground control points (GCPs) within processing pipelines, which can otherwise significantly limit the speed, cost and efficiency of 3D reconstruction methods. Terrestrial and Unmanned Aerial Systems-based photogrammetry are well established and efficient geospatial techniques for detailed 3D documentation and reconstruction, but GCPs are still required to achieve the highest level of accuracy in georeferenced geometric surveys (Nex and Remondino, 2014). Following advancements in imaging rover technology (Baiocchi et. al., 2018) and supported by various investigations into GNSS-assisted terrestrial photogrammetry (Nocerino et al., 2012; Forlani et al., 2014; Jaud et al., 2020; Morelli et al., 2022; Previtali et al., 2023; Eker, 2023; Oniga et al., 2024), commercial integrated sensor solutions are now readily available. One such solution is the Leica Geosystems GS18i that integrates a Global Navigation Satellite System (GNSS) receiver with an Inertial Measurement Unit (IMU) and an imaging sensor (Leica GS18i, 2024). The concept behind the GS18i instrument is that it can use 3D imaging to measure distant points within a survey area that are otherwise not measurable with a conventional GNSS receiver (e.g. points on the façade of a building). Imagery can be continuously acquired while surveying accessible points of interest using the Real Time Kinematic (RTK) and/or the Precise Point Position (PPP) GNSS capabilities of the instrument. Unlike traditional GNSS receivers that necessitate a vertical survey pole during observation, the GS18i features a tilt compensator, thereby enabling image acquisition from various angles. Imagery is then photogrammetrically orientated (SLAM) using camera positions calculated on-the-fly during fieldwork using the GNSS/IMU integrated solution. Alternatively, GCPs can be incorporated as external constraints for solving a photogrammetric bundle adjustment (James et al., 2019). Over recent years, several studies have investigated the capabilities of the GS18i, e.g. in simple urban settings (Casella et al., 2021), for glacier monitoring with UAV data (Belloni et al., 2022) and under forest canopies (Wan et al., 2024). However, to our knowledge, no investigation evaluated the 3D geometric accuracy of the GS18i system in comparison to different processing methodologies and tools.

1.1 Aim of the paper

This research aims to assess the geometric potential of the Leica Geosystems GS18i visual positioning system for 3D reconstruction purposes using different processing pipelines in various surveying scenarios. Processing pipelines, including a photogrammetric self-calibrating bundle adjustment with camera GNSS positions as constraints and a classical approach with the use of a minimal number of GCPs, are assessed using data collected using the GS18i in RTK and PPP GNSS modes. Accuracy is evaluated with reference to independent check points (ICPs) in each study area. The GS18i is used for 3D documentation and mapping purposes and its performance compared to conventional photogrammetric methods using a digital single-lens reflex (DSLR) camera.

2. STUDY AREAS

2.1 Study site 1: Vindolanda Roman Fort

The first study area is Vindolanda Roman Fort (Vindolanda, 2024), located north of the modern-day village of Bardon Mill, Northumberland, approximately 35 miles west of Newcastle upon Tyne (UK). The site was a garrison occupied by the Roman Empire between c. 85 and 350 AD. Today the fort is in the care of the Vindolanda Trust and is one of the most important archaeological locations along the UNESCO World Heritage Site of Hadrian's Wall (2024). The fort is most notably famed for the Vindolanda Tablets which, at the time of their discovery in 1973, were the oldest known surviving handwritten documents in Britain (Vindolanda tablets online, 2024). Vindolanda has undergone extensive excavation since the 1930s and significant stonework is exposed, including the area surveyed in this research (Figure 1). Sites along Hadrian's Wall (e.g. Fieber et al., 2017) are subject by both natural (e.g. Magna Roman Fort; Guiney et al., 2021) and anthropogenic impacts (e.g. Sycamore Gap; Morelli et al., 2024), with geospatial techniques offering value for reconstruction and visualisation (Rodriguez-Gonzalvez, 2017), leading to sustainable cultural heritage (Xiao et al. 2018).

Figure 1. (a) Test field target distribution around Vindolanda Roman Fort study area visualized on an orthoimage generated with a DJI Phantom 4 RTK. (b, c) Example imagery captured using the GS18i of the study area, including GCP/ICP targets.

Figure 2. (a) Test field target distribution on the façade of The Arches (Newcastle University campus), illustrated with a dense point cloud generated using Canon SLR imagery. Imagery of the façade captured by the (b) Canon and (c) GS18i over GCP 125, located at the corner of an air brick.

2.2 Study site 2: The Arches

The Quadrangle Gateway ("The Arches") is a three-storey building at the heart of Newcastle University campus (Figure 2a) designed by Newcastle-born architect William Henry Knowles (1857-1943). The Arches were built in 1911 to provide a gateway from King's Road into the Quadrangle and access to the Armstrong Building, the original site of Armstrong College which was founded in 1871 and later became Newcastle University (The Arches, 2024). Above the Arches is a recessed statue of King Edward VII (1841-1910). As a building of special interest, since 1987 the gateway has been afforded protection as a Grade II listed building on the National Heritage List for England (Historic England, 2024). The Arches has been used as a study site for previous geospatial-cultural heritage research (e.g. Dhonju et al., 2018).

3. METHODS AND DATASETS

3.1 Overview of methodological workflow

In this study, we aim to assess the accuracy of a mobile visual positioning device integrated with RTK and PPP technologies – the Leica GS18i - for surveying characteristic points of buildings or heritage sites without the use of GCPs. The acquired data is processed using both Agisoft Metashape (2023) and Leica Geosystems' Infinity (2024). Infinity is specifically designed to jointly process GNSS/IMU and imagery datasets (Leica Infinity, 2024). This approach is compared to a traditional photogrammetric survey conducted with a DSLR camera and GCPs. Table 1 summarises the various self-calibrating bundle adjustment tests conducted on GS18i datasets, also indicating the software used in each test. Tests V1 and A1 relied on camera exposure stations, i.e., free network solutions with a final BA constraining camera poses on the observed RTK/PPP positions. The latter two tests incorporated control information in the object space, i.e., constrained network solutions with a limited number of GCPs. Specifically, in Test V3, three GCPs were used at Vindolanda (GCPs 1, 2, and 4; Figure 1) and in Test A3 four GCPs were located on the façade of the Arches (GCPs 105, 107, 120, and 125; Figure 2a). Test A2 assessed the GS18i's performance by combining the GNSS constraints on camera positions with a single GCP (GCP 116; Figure 2), which was not included in Test A1. Similarly, one single GCP (GCP 2; Figure 1a) was used in Test V2, at Vindolanda. For the Arches, a separate set of nine ICPs was used for accuracy assessment; however, this was not possible for the Vindolanda experiment due to the limited number of coordinated points available. A bundle optimisation with GCPs was applied to the benchmark DSLR dataset in both study areas. Error assessment included the calculation of root mean square errors (RMSEs) and standard deviations (STDs) at ICPs, as well as the mean reprojection errors (MREs) provided by the two software packages.

Additionally, and specifically for the Arches, an additional relative error assessment included RMSEs on 5 scaled distances, which were calculated between five pairs of ICPs for the Arches (100-108, 101-104, 104-117, 117-121, 121-123; Figure 2a), and three scaled distances for Vindolanda (1-2, 2-4, 4-2).

ID	*Process*	*GCP/ICP*	*Infinity*	*Metashape*
Vindolanda				
Test V1	Optimised on cameras with lever arm calibration	0/6	X	X
Test V2	Optimised on cameras with 1 GCP	1/5	-	X
Test V3	Bundle optimisation with 3 GCPs	3/3	X	X
Arches				
Test A1	Optimised on cameras with lever arm calibration	0/9	X	X
Test A2	Optimised on cameras with 1 GCP	1/9	-	X
Test A3	Bundle optimisation with 4 GCPs	4/9	X	X

Table 1. Testing and analyses performed using the GS18i. GCP: Ground Control Points; ICP: Independent Check Points.

3.2 Vindolanda dataset

Two photogrammetric datasets were acquired around a stonework structure at Vindolanda on 17th April 2024. The first dataset followed a conventional photogrammetric camera network using a Canon EOS 6D Mark II DSLR camera. This consisted of 108 images acquired with the full-frame sensor (35.9 x 24.0 mm), fitted with a Sigma 35 mm f/1.4 DG HSM lens, resulting in 6240×4160 pixel (26 Mpix) images. The second dataset (Figure 1b-c) was acquired with the GS18i visual positioning system in RTK mode. This used a Leica Geosystems AR0135 camera with a 3.10 mm nominal focal length and 0.0037 mm pixel size (Leica GS18i, 2024), resulting in 349 images at 1280 x 960 (1.2 Mpix) pixels. The Canon photogrammetric solution serves as the benchmark with which to compare the GS18i solutions.
Moreover, one GNSS reference station was established at the study site and surveyed for 3 hours 37 minutes using an independent Leica GS10 receiver. The reference station was coordinated using static GNSS, delivering sub-cm level 3D accuracy relative to a local UK network base station (CARL) in Ordnance Survey Great Britain 36 (OSGB36) and Ordnance Datum Newlyn (ODN). Six b/w circular targets, used as GCP/ICPs, were coordinated with respect to the established GNSS reference station, using 3 minutes of GNSS data per point with a second independent Leica GS10 receiver.

3.3 Arches dataset

Four image datasets were acquired of the façade of the Arches with (1) 214 images with the GS18i RTK on 18th October; (2) 38 images with the Canon EOS 6D Mark II DSLR camera on 24th October; (3) 156 images with the GS18i PPP on 31st October 2024; and (4) 192 images with the GS18i RTK, also on 31st October 2024. Acquisition in RTK mode was performed twice to assess repeatability. The Canon camera and lens were identical to those used for the Vindolanda dataset (Section 4.1), and Canon imagery was also used as the benchmark dataset for this study area. According to Historic England's standard specifications on geospatial surveys for photogrammetric datasets, a ground sampling distance (GSD) of 0.002 m is sufficient to achieve an output scale of 1:50 for cultural heritage buildings (Section 4.4.2 in Historic England standards (2024)). In line with these specifications, capturing images with a Canon camera (assuming a 35 mm focal length and a 5.79 µm pixel size) from a distance of 10 m from the façade produced a GSD of 0.002 m and allowed for coverage of the façade's full height (Figure 2a).
As opposed to the Vindolanda study area, establishing b/w targets on the façade of the Arches was challenging due to permission requirements. For that reason, manmade features were identified, e.g. the corners of airbricks (Figure 2b-c), which were discernible on both Canon and GS18i imagery. While 30 manmade features were identified and surveyed, only 15 were used in the experiments presented here, as some were not visible in all image datasets. For consistent comparative analysis only features with at least four image projections in all datasets were retained. For that reason, features 113 and 116, shown in Figure 2a, were excluded from the final results.

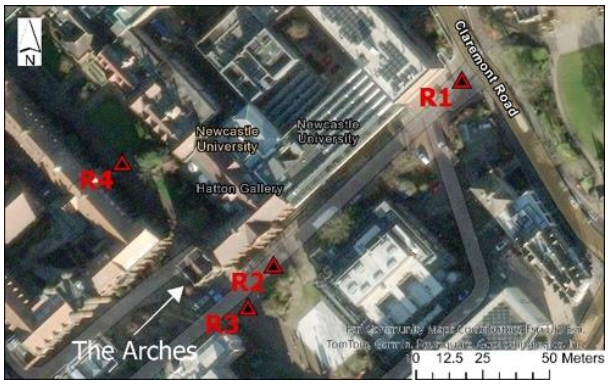

Figure 3. Overview of the four GNSS reference stations at the Arches use case.

Four GNSS reference stations were established at the study site (R1-4; Figure 3) and each surveyed for 1 hour using a Leica GS10 receiver in static GNSS mode on 16th October 2024. These reference stations were coordinated relative to a local UK network base station (NCAS) in OSGB36-ODN, achieving sub-cm-level 3D accuracy, using Infinity. The reference stations were then used to survey the manmade features on the façade with a Leica total station on 18th October 2024. 14 of the 15 features were surveyed from both R2 and R3 reference stations, yielding an average difference of 0.001 m in Easting, Northing, and Height. 15 observations of the façade's manmade features from the R3 reference station were subsequently used as reference coordinates for GCPs/ICPs in all experiments (Figure 2a). As seen in Figure 3, R3 was positioned directly in front of the façade, enabling selection of the most suitable manmade features.
Prior to image capture, an additional test was conducted on 31st October 2024 to assess the 3D quality of the RTK and PPP GS18i solutions on point measurement precision at the four reference stations (R1-4; Figure 3). It should be noted that to perform GNSS integer ambiguity resolution in real-time, RTK relies on GNSS-based corrections from a nearby reference station, in this case from the Leica SmartNet GNSS network. However, PPP is not dependent on any reference station, and it can be used without being connected to a GNSS network. Instead, PPP real-time corrections are calculated using GNSS orbital information, hence PPP mode can be used anywhere. It should be noted that Leica subscriptions were required for access to RTK and PPP modes.

3.4 Image capture with the GS18i

The GS18i system captures images only when GNSS RTK/PPP corrections are available in real-time. During fieldwork, it is operated using Leica's Captivate surveying software (Leica Captivate, 2024). Once RTK/PPP corrections are established, the

operator, with the GS18i mounted on a surveyor's pole, slowly walks along while capturing images. The system captures multiple images within a 60-second period, storing them as a single image group in Leica Captivate. If the RTK/PPP signal is lost, image capture automatically stops. Leica Captivate also provides a quality indicator for each image group, reflecting factors such as satellite count, satellite constellation, and GNSS RTK/PPP signal quality at the time of data capture.

A significant challenge encountered during image collection at the Arches was the loss of the RTK/PPP link at distances closer than c. 4 - 5 m from the façade. This was caused by the tall buildings surrounding the Arches on the university campus, which created a typical urban canyon environment with poor GNSS signal quality. Multiple attempts were made during fieldwork on 18th October to capture the highest quality images possible. Table 2 lists the quality indicators provided by Leica Captivate for each image group selected for the experiments presented herein.

Study site/GNSS mode	*Date (2024)*	*Image group*	*#Images*	*Quality [m]*
Vindolanda/RTK	17/04	01	118	0.025
		02	116	0.020
		03	115	0.027
Arches/RTK1	18/10	09	115	0.076
		10	99	0.116
Arches/RTK2	31/10	01	117	0.115
		02	75	0.145
Arches/PPP	31/10	01	42	0.259
		04	114	0.187

Table 2. Quality indicated by Leica Captivate.

Table 2 suggests a one-order-of-magnitude difference in RTK image capture quality between Vindolanda and the Arches, attributed to Vindolanda's open sky environment compared to the GNSS-limited urban setting of Newcastle University campus. Between image groups in the two RTK experiments, a maximum discrepancy of 6.9 cm was observed (internal metric provided by the Leica software). Additionally, there was a notable quality difference between PPP and RTK solutions, with a maximum discrepancy of 18.3 cm (Table 2), with PPP delivering the lowest accuracy. However, before capturing images, the PPP solution was allowed to converge for five minutes at a fixed point, achieving approximately 6 cm accuracy in 3D, as reported in Leica Captivate.

3.5 Software analysis

Images stored in Leica Captivate do not include the RTK/PPP real-time coordinates embedded in the EXIF file. For that reason, analysis in Infinity firstly involved the extraction of the GNSS camera positions observed with the GS18i that have been consistently applied across the two software packages. Secondly, the image pixel measurements of the marked targets visible on GS18i imagery were shared across both software packages for all bundle adjustment tests. The "OPENCV" camera calibration model was adopted, comprising focal length (fx, fy), principal point (cx, cy), two radial distortion (k1, k2), and two tangential distortion (p1, p2) parameters. According to Infinity's log files, the OPENCV scale-invariant feature transform (SIFT; Lowe, 2004) algorithm is adopted for image matching. In Metashape and Infinity, point marking accuracy was configured at 0.5 pixels for Vindolanda and 1 pixel for the Arches. This is because the b/w targets in Vindolanda enabled sub-pixel accuracy, which was higher than that achieved with the manmade features on the façade. Given the sub-cm surveying absolute accuracies at GCPs/ICPs, 2D and 1D control point accuracies were set to 0.010 m and 0.020 m, respectively, for all datasets in both software. It is worth noting that lever arm calibration was applied in Tests V2, A2 and V3, A3 (Table 1) in Metashape; while it is assumed to be implemented in Infinity, this is not explicitly confirmed in the software manual. Tests without lever arm calibration were also applied in Metashape but are not presented in this research.

4. RESULTS

4.1 GS18i point measurement precision

Table 3 shows the residuals for Easting (E), Northing (N), and Height (H), calculated from GNSS-static surveyed coordinates after four observations using the GS18i in RTK/PPP modes at each of the four reference stations. For RTK point measurements, consistency was maintained at a cm-level for Easting and Northing, with a maximum discrepancy of 3 cm in Height. The STDs were of similar magnitude in plan, with a maximum of 0.011 m in Height. In PPP mode, although the STD estimations showed a similar cm-level consistency, a noticeable systematic offset appeared, with a ca 12 cm shift in plan and a ca 10 cm difference in Height across the four reference stations. The PPP statistics on point measurement precision may also account for the ca 20 cm 3D quality observed in the image capture on the same day (Table 2), though the method used by Leica Captivate to estimate this quality measure remains unclear.

	mean residuals [m]			*STD [m]*		
#	*E*	*N*	*H*	*E*	*N*	*H*
RTK						
R1	-0.004	0.011	0.014	0.004	0.010	0.011
R2	0.001	0.003	-0.011	0.000	0.001	0.007
R3	0.008	0.006	-0.022	0.001	0.003	0.007
R4	0.014	-0.005	-0.030	0.003	0.005	0.002
PPP						
R1	0.128	0.083	-0.013	0.010	0.029	0.036
R2	0.126	0.125	-0.008	0.006	0.025	0.016
R3	0.125	0.104	-0.103	0.001	0.005	0.016
R4	0.084	-0.108	-0.006	0.008	0.009	0.018

Table 3. Quality statistics at the four GNSS reference stations.

4.2 Error evaluation overview

Table 4 presents the RMSEs and STDs for the three coordinate axes and Figure 4 shows the equivalent 3D RMSEs on ICPs across all experiments. When comparing the overall RTK planimetric results between Vindolanda and the Arches in Infinity, one might anticipate lower RMSEs in the open area. However, this expectation is only partially met; the RMSE in Easting at Vindolanda is 1.5 times higher than that at the Arches. Additionally, the RMSE in Height at Vindolanda is six times greater than the RMSEs in both Easting and Northing. In terms of absolute accuracies, the Canon photogrammetric datasets processed in Metashape achieved the highest accuracy and consistency, with RMSEs and STDs under 1.6 cm across all three coordinate axes. A 1.8 cm 3D RMSE estimated at the Arches (Test A3 – Bench; Figure 4) and a 1.7 cm 3D RMSE estimated at Vindolanda (Test V3 – Bench; Figure 4). The closest results to this benchmark were achieved with Metashape on RTK 1 and 2 at the Arches, when GNSS camera positions and a single GCP were optimised in the bundle adjustment (Tests A2 RTK 1/2) and with Metashape on Test A1 RTK 1 (Figure 4). The tests conducted in Metashape using the Canon produced 3D RMSEs below 2 cm, whereas those with the GS18i resulted in accuracies exceeding 2 cm (Figure 4).

Test	*Metashape – RMSE [m]*			*Metashape – STD [m]*			*Infinity – RMSE [m]*			*Infinity – STD [m]*		
	E	*N*	*H*	*E*	*N*	*H*	*E*	*N*	*H*	*E*	*N*	*H*
Vindolanda - RTK GS18i												
V1	0.025	0.021	0.032	0.012	0.007	0.009	0.028	0.016	0.015	0.019	0.011	0.008
V2	0.016	0.022	0.013	0.012	0.012	0.011	-	-	-	-	-	-
V3	0.012	0.021	0.013	0.014	0.025	0.016	0.024	0.015	0.011	0.028	0.015	0.013
Vindolanda – Benchmark Canon												
V3	0.004	0.016	0.004	0.005	0.010	0.005	-	-	-	-	-	-
Arches - RTK 1 GS18i												
A1	0.011	0.020	0.011	0.012	0.021	0.012	0.018	0.014	0.063	0.019	0.014	0.008
A2	0.011	0.020	0.011	0.012	0.020	0.011	-	-	-	-	-	-
A3	0.009	0.027	0.009	0.010	0.027	0.010	0.020	0.015	0.012	0.021	0.013	0.008
Arches - RTK 2 GS18i												
A1	0.024	0.017	0.020	0.012	0.018	0.013	0.017	0.021	0.017	0.018	0.016	0.013
A2	0.014	0.014	0.018	0.012	0.015	0.014	-	-	-	-	-	-
A3	0.017	0.025	0.013	0.015	0.021	0.012	0.017	0.020	0.014	0.018	0.017	0.014
Arches – PPP GS18i												
A1	0.223	0.260	0.494	0.053	0.073	0.050	0.103	0.226	0.068	0.073	0.099	0.064
A2	0.061	0.151	0.073	0.050	0.148	0.072	-	-	-	-	-	-
A3	0.025	0.021	0.012	0.020	0.017	0.012	0.105	0.221	0.059	0.086	0.119	0.062
Arches – Benchmark Canon												
A3	0.013	0.011	0.007	0.012	0.011	0.007	-	-	-	-	-	-

Table 4. Error evaluations with RMSEs and STDs on ICPs, as defined in Table 1, for all experiments.

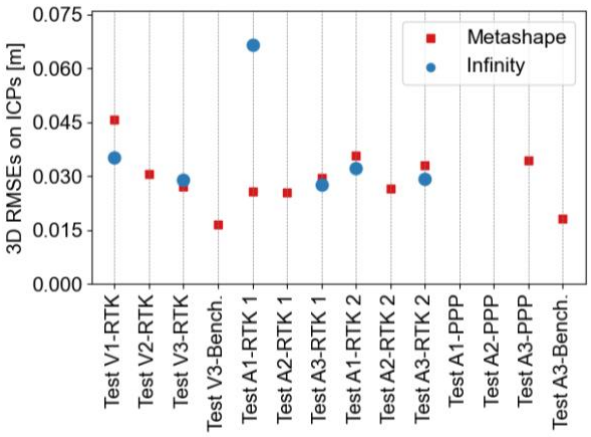

Figure 4. 3D RMSEs on ICPs for all tests as in Table 4.

Tests performed in PPP mode showed the lowest absolute accuracies, especially in Infinity, due to a systematic offset of approximately 0.100 m in Easting and 0.200 m in Northing, consistent with the point measurement precision on that day (Table 3). For that reason, these results were not included in Figure 4, as they exceeded the maximum value of the y-axis.

4.3 Error evaluation with regards to constraints

Including a minimum number of GCPs generally improved RMSE values across most tests in both software packages. However, as shown in Table 4 and Figure 4, the improvement in Infinity was not as substantial as in Metashape between Tests V1, A1 and V3, A3. For example, in Test V3 of the RTK experiments, RMSEs and STDs remained within a similar range of two to three cm across all three coordinate axes. This is further demonstrated in Figure 4, where the 3D RMSEs in Infinity (Tests V1-V3 and A1-A3 RKT 2) fall within the range of two to four cm. Although Infinity employs a SIFT-like variant similar to Metashape, the optimisation process for bundle adjustment when incorporating GCPs remains unclear. Results in Table 4 suggest that Infinity's optimisation primarily depended on the initial image orientation obtained through RTK/PPP GNSS observations. Consequently, in the PPP experiment, the addition of four GCPs in Test A3 did not improve RMSEs. As opposed to Metashape result for the Test A3 PPP where GCPs significantly improved the accuracy to 3.4 cm in 3D (Figure 4).

The mean reprojection errors (MREs) calculated on ICPs were at the sub-pixel level in most experiments conducted in Metashape, except for the PPP, but were significantly higher in Infinity (Table 5). This further highlights the differences in how the two software programs implement bundle adjustment. However, a notable reduction in MREs was observed in Infinity from Test A1 RTK 1 to Test A3 RTK 1 as well as from Tests V1 to V3. Specifically, the addition of three and four GCPs resulted in MRE improvements of 2 pixels at Vindolanda and 6 pixels at the Arches. Regardless of GCP inclusion, the analysis in Infinity indicated that ICP 101 (Figure 2a) consistently produced high reprojection errors (e.g. 9 pixels in Test A1 RTK 2), resulting in relatively elevated RMSEs in height across all tests. In PPP experiments, due to relatively high systematic errors, the 3-pixel difference between Tests A1 and A3 could not be considered a true improvement, given the MRE remains around 20 pixels (Table 5).

In contrast, Metashape successfully eliminated the systematic bias in PPP experiments when four GCPs were included in the bundle optimisation. This improvement is evident in both the absolute (Table 4 and Figure 4) and relative error checks (Table 5). For absolute error evaluation, the initial 20 cm bias in Easting and Northing and 50 cm in Height seen in Test A1 PPP decreased to 2.5 cm (Easting and Northing) and 1.2 cm (Height) in Test A3 (Table 4). In other words, the initial 3D RMSE of 60.1 cm improved by 18%, resulting in a 3D RMSE of 3.4 cm (Figure 4) in Test A3 PPP, comparable to Test A1 RTK 2 results achieved without GCPs. Incorporating a single GCP in Test A2 led to a considerable reduction in RMSEs for the PPP experiment, though a 15 cm bias remained in the Northing direction (see RMSE and STD in Table 4). For relative error checks, no substantial improvement in RMSEs on scale bars was observed with the addition of GCPs, except in the PPP experiment (Table 5). Specifically, the relative accuracy improved from 6.7 cm to

2.9 cm, which is close to the average RMSE on scale bars of 2.2 cm across all RTK experiments at the Arches.

Test#	*RMSE on scale bars [m]*	*MRE [pixel]*	*MRE [pixel]*
	Metashape		*Infinity*
Vindolanda - RTK GS18i			
V1	0.020	0.5	4.2
V2	0.029	0.4	-
V3	0.040	0.5	2.0
Arches - RTK 1 GS18i			
A1	0.023	0.7	8.7
A2	0.023	0.8	-
A3	0.025	0.8	2.4
Arches - RTK 2 GS18i			
A1	0.019	0.7	3.0
A2	0.019	0.7	-
A3	0.024	0.7	2.5
Arches - PPP GS18i			
A1	0.063	0.9	26.0
A2	0.067	0.7	-
A3	0.029	1.0	23.9

Table 5. Scale bar assessment and mean reprojection errors on ICPs for GS18i experiments.

Regarding the RTK experiments, Figure 4 presents box plots of the residual variances, as calculated from the differences between surveyed and estimated coordinates at ICPs for both software solutions. Figure 5 displays the inconsistency between the two software processes. In Test A1 RTK 2, there was a considerate overestimation in Easting with Metashape and in Northing with Infinity. Such discrepancies could be attributed to the different processes the two software apply, as previously mentioned. However, apart from the outlier of 6.3 cm in Height (Test A1 RTK 1 Table 4), the box plot's interquartile ranges were within ± 2.5 cm (Figure 5), relatively consistent with the RMSEs on scale bars, seen in Table 5.

For the estimated ground sample distance (GSD), tests with the Canon benchmark dataset achieved approximately 1 mm GSD in both study areas. This surpassed the expectations outlined in Section 3.3 for achieving an output scale of 1:50 for cultural heritage buildings, as in the case of the Arches. For the GS18i, Infinity produced GSD values of 23 mm at Vindolanda and 29 mm at the Arches. The GS18i sparse point cloud and image orientation from Tests V3 and A3 RTK 2 are shown in Figure 6.

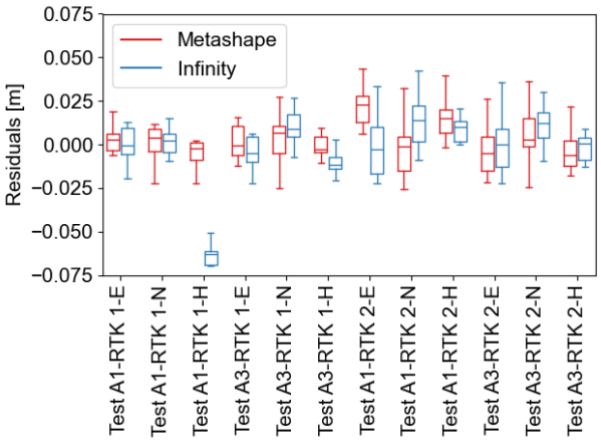

Figure 5. Box plots of residuals in Easting (E), Northing (N) and Height (H) on ICPs of RTK Tests A1 and A3.

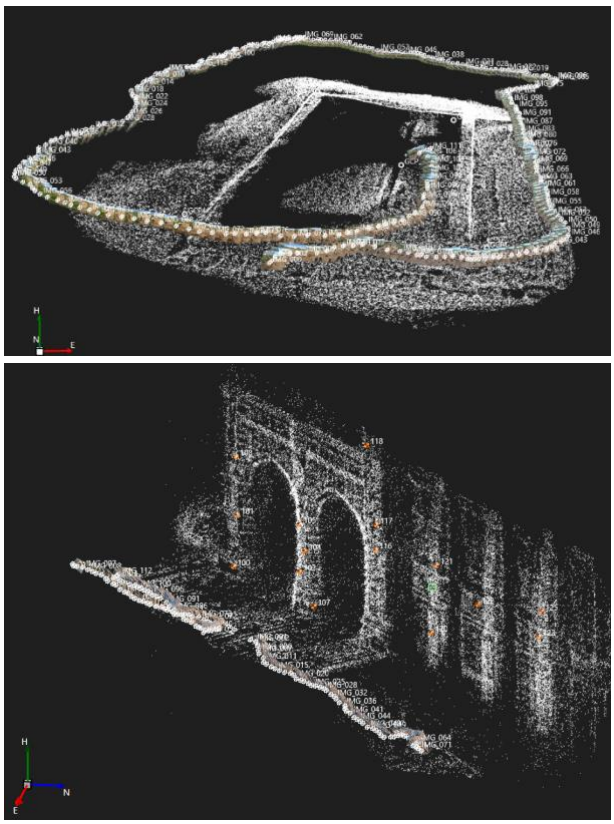

Figure 6. GS18i image orientation and sparse point cloud generated with Infinity at Vindolanda (top) and the Arches (bottom).

5. DISCUSSION

Investigations of the presented study showed that the GS18i system in RTK mode and Infinity could deliver a 3.2 cm 3D absolute accuracy without the use of GCPs even in poor GNSS signal conditions (Test A1 RTK 2; Figure 4). The best accuracy achieved in this study surpassed the levels reported by Casella et al. (2021). Specifically, Casella et al. (2021) utilised the GS18i system in RTK mode and reported RMSEs of 4.5 cm, 2.5 cm, and 6.6 cm in Easting, Northing, and Height, respectively, with their analysis conducted in Infinity. However, they did not report reprojection errors, which were relatively high in the present study using Infinity. One of the primary reasons for the high reprojection errors, especially when the bundle was optimised with GCPs, was the insufficient baseline quality between image pairs. When walking along the façade at the Arches with the GS18i the manmade features on the wall were viewed multiple times from the same angle. That was not exactly the case at Vindolanda, as b/w targets were viewed from multiple directions since the image capture network was circular and not linear as in of the case of the Arches façade (Figure 6). Although the tilt compensator of the GS18i system was utilised during image capture, the low image resolution of the sensor made it difficult to clearly identify manmade features in oblique images compared to those captured directly in front of the façade, hence the insufficient baseline quality.

The study also revealed discrepancies in results between Metashape and Infinity. While the specifics of Infinity's bundle adjustment optimisation remain unclear, it was less effective than Metashape in improving accuracies when GCPs were incorporated into the process. Additionally, Infinity's optimisation failed to significantly reduce the high reprojection errors (Table 5). The requirement for a minimum of three GCPs

to run a bundle adjustment in Infinity may indicate that the process primarily applies a Helmert transformation, and heavily relies on the initial RTK/PPP image orientation, which could explain the minimal changes in RMSEs between Tests V3 and V1 (Table 4). Notably, Metashape achieved the highest accuracies (approximately 2.5 cm 3D RMSE) in Tests A2 RTK1 and 2 (Table 5, Figure 4) when the initial image orientation was relatively accurate, excluding PPP. This was accomplished by including a single GCP, an operation that was not possible in Infinity.

It might have been expected to achieve better accuracies at Vindolanda compared to the Arches, given the restricted GNSS signal conditions. However, this was not the case for any of the software. Surprisingly, better accuracies were achieved at the Arches, despite the absence of b/w targets. This is likely due to the limited number of targets and fewer projections at Vindolanda, as the targets were placed on the ground and appeared too oblique in some images. Additionally, lever arm calibration was applied in Metashape for all experiments, which may have contributed to the relatively higher RMSEs at Vindolanda compared to the Arches. An attempt without lever arm calibration yielded lower RMSEs at Vindolanda; however, this was excluded from the presented work to maintain consistency. Future research will explore lever arm calibration in greater detail.

During fieldwork, the 3D image quality indicator (Table 2) calculated in Leica Captivate proved helpful, particularly in the PPP experiments, where it highlighted high values for specific image groups. At Vindolanda, the image quality indicator provided a realistic estimation of uncertainty, suggesting that the captured image groups could not achieve better than 2.7 cm accuracy (Table 2). This aligned with the resulting 3D accuracy of 3.5 cm in Infinity for Test V1 (Figure 4, Table 4). However, this consistency was not observed in the RTK experiments at the Arches. Despite the image quality indicators showing an uncertainty of approximately 11 cm, the resulting 3D accuracies in Infinity were below this figure, even without including GCPs.

It is worth noting that the GS18i system is designed for efficient field operation, particularly for capturing detailed measurements in areas with poor GNSS signal conditions. To demonstrate this capability, measurements of two manmade features (101 and 103; Figure 2a) were taken in Leica Captivate using the image group captured closest to the façade during an attempt on 18th October 2024. A 3D RMSE of 9 cm was achieved for these features, based on five image projections. Further processing in Infinity showed improved accuracies in the RTK 1 experiments. Because of the low resolution and the challenge of accurately selecting the correct feature in Leica Captivate, we excluded such observations from this study.

6. CONCLUSIONS

This study has presented investigations into the 3D geometric accuracy of the Leica GS18i visual positioning system in both open environments and complex conditions with poor GNSS signal quality. Using Leica's proprietary software in RTK mode without ground control points (GCPs), 3D RMSEs ranging from 3.2 cm to 3.5 cm were achieved when compared to independently surveyed ICPs. The research also conducted a comparative analysis using the same dataset in Metashape and Infinity, alongside a benchmark validation with a Canon DSLR dataset processed through conventional photogrammetry. The findings have showed that Metashape effectively reduced high reprojection errors and systematic bias in PPP mode, achieving 3D RMSEs of 3.4 cm (in PPP) and 2.5 cm (in RTK) with the integration of a single GCP and camera optimisation. Further studies of the GS18i system's capabilities include repeated experiments in GNSS PPP mode and comparisons with other low-cost GNSS-assisted terrestrial photogrammetric systems.

ACKNOWLEDGEMENTS

Survey work involved the EPSRC Centre for Doctoral Training (CDT) in Geospatial Systems (EP/S023577/1) and was conducted using instrumentation provided by UKCRIC – UK Collaboratorium for Research in Infrastructure & Cities: Newcastle Laboratories (EP/R010102/1). Thanks are due to the Vindolanda Trust and Leica Geosystems for supporting the Vindolanda field campaign. Special thanks are given to James Whitworth and Shanmukh Gollapudi from Leica Geosystems for their valuable consultation. We would also like to thank Frank Atkinson, James Goodyear and Joe Haines from Newcastle University, as well as Sean Ince and Chenyu Xue from The University of Nottingham, for their support during fieldwork.

REFERENCES

AgiSoft Metashape (2024). http://www.agisoft.com/

Baiocchi V., Piccaro C., Allegra M., Giammarresi V., Vatore F., 2018., Imaging rover technology: characteristics, possibilities and possible improvements. *J. Phys., Conf. Ser.*, 1110(1), 012008

Belloni V., Fugazza D., Di Rita M., 2022. UAV-based glacier monitoring: GNSS Kinematic track post-processing and direct georeferencing for accurate reconstructions in challenging environments. *Int. Arch. Photogramm. Remote Sens. Spatial Inf. Sci., XLIII-B1,* 367-373.

Casella, V., Franzini, M. and Manzino, A.M., 2021. GNSS and Photogrammetry by the same Tool: a First Evaluation of the Leica GS18I Receiver. *Int. Arch. Photogramm. Remote Sens. Spatial Inf. Sci., XLIII-B2,* 709-716, doi.org/10.5194/isprs-archives-XLIII-B2-2021-709-2021.

Dhonju, H., Xiao, W., Mills, J. and Sarhosis, V., 2018. Share Our Cultural Heritage (SOCH): Worldwide 3D Heritage Reconstruction and Visualization via Web and Mobile GIS. *ISPRS International Journal of Geo-Information,* 7 (9): 360.

Eker, R., 2023. Comparative use of PPK-integrated close-range terrestrial photogrammetry and a handheld mobile laser scanner in the measurement of forest road surface deformation. *Measurement*, *206*, p.112322.

Fieber, K.D., Mills, J.P., Peppa, M.V., Haynes, I., Turner, S., Turner, A., Douglas, M. and Bryan, P.G., 2017. Cultural heritage through time: a case study at Hadrian's Wall, United Kingdom. *International Archives of Photogrammetry, Remote Sensing and Spatial Information Sciences*, 42(2/W3): 297–302.

Forlani, G., Pinto, L., Roncella, R. and Pagliari, D., 2014. Terrestrial photogrammetry without ground control points. *Earth Science Informatics*, *7*, pp.71-81.

Guiney, R., Santucci, E., Valman, S., Booth, A., Birley, A., Haynes, I., Marsh, S. and Mills, J., 2021. Integration and analysis of multi-modal geospatial secondary data to inform management of at-risk archaeological sites. *ISPRS International Journal of Geo-Information*, 10(9): 575.

Historic England, 2024. Quadrangle Gateway "The Arches" listed building. https://historicengland.org.uk/listing/the-list/list-entry/1024828, last accessed 04/11/2024.

Historic England standards, 2024. Geospatial survey specification guidelines for cultural heritage. Geospatial Survey Specifications for Cultural Heritage, last accessed 04/11/2024.

Hadrian's Wall, 2024. UNESCO World Heritage Site, Frontiers of the Roman Empire, https://whc.unesco.org/en/list/430/.

Jaud, M., Bertin, S., Beauverger, M., Augereau, E. and Delacourt, C., 2020. RTK GNSS-assisted terrestrial SfM photogrammetry without GCP: Application to coastal morphodynamics monitoring. *Remote Sensing*, *12*(11), p.1889.

James, M. R., Chandler, J. H., Eltner, A., Fraser, C., Miller, P. E., Mills, J. P., Noble, T., Robson, S., Lane, S. N., 2019. Guidelines on the use of structure-from-motion photogrammetry in geomorphic research. *Earth Surface Processes and Landforms*, 44(10), 2081-2084.

Leica Captivate, 2024. Surveying Field Software, https://leica-geosystems.com/products/total-stations/software/leica-captivate, last accessed 05/11/2024.

Leica GS18i, 2024. GNSS RTK Rover with Visual Positioning receiver by Leica Geosystems AG. https://leica-geosystems.com/products/gnss-systems/smart-antennas/leica-gs18i, last accessed 05/11/2024.

Leica Infinity, 2024, Leica Geosystems Development Team, Software. https://leica-geosystems.com/products/gnss-systems/software/leica-infinity.

Lowe, 2004. Distinctive Image Features from Scale-Invariant Keypoints. *Int. Journal of Computer Vision*, 60, 91-110.

Metashape, 2023. User manual professional edition, version 1.5, https://www.agisoft.com/pdf/metashape-pro_1_5_en.pdf, last accessed 10/01/2023.

Morelli, L., Menna, F., Vitti, A., Remondino, F., 2022. Action cams and low-cost multi-frequency antennas for GNSS assisted photogrammetric applications without ground control points. *Int. Arch. Photogramm. Remote Sens. Spatial Inf. Sci.*, XLVIII-2/W1-2022, 171-176.

Morelli, L., Mazzacca, G., Trybała, P., Gaspari, F., Ioli, F., Ma, Z., Remondino, F., Challis, K., Poad, A., Turner, A., and Mills, J. P., 2024. The Legacy of Sycamore Gap: The Potential of Photogrammetric AI for Reverse Engineering Lost Heritage with Crowdsourced Data. *Int. Arch. Photogramm. Remote Sens. Spatial Inf. Sci.*, XLVIII-2-2024, 281-288.

Nex F., Remondino, F., 2014: UAV for 3D mapping applications: a review. *Applied Geomatics*, Vol.6(1), pp. 1-15.

Nocerino, E., Menna, F. Remondino, F., 2012. GNSS/INS aided precise re-photographing. Proc. 18th IEEE Int. Conference on Virtual Systems and Multimedia – VSMM, pp. 235-242.

Oniga, E., Boroianu, B., Morelli, L., Remondino, F., and Macovei, M., 2024. Beyond ground control points: cost-effective 3D building reconstruction through GNSS-integrated photogrammetry. *Int. Arch. Photogramm. Remote Sens. Spatial Inf. Sci.*, XLVIII-2/W4-2024, 333-339.

Previtali, M., Barazzetti, L., Roncoroni, F., Cao, Y. and Scaioni, M., 2023. 360° Image Orientation and Reconstruction with Camera Positions Constrained by GNSS Measurements. *Int. Arch. Photogramm. Remote Sens. Spatial Inf. Sci.*, 48, pp.411-416.

Rodriguez-Gonzalvez, P., Munoz-Nieto, A.L., Del Pozo, S., Sanchez-Aparicio, L.J., Gonzalez-Aguilera, D., Micoli, L., Gonizzi Barsanti, S., Guidi, G, Mills, J., Fieber, K, Haynes, I. and Hejmanowska, B., 2017. 4D reconstruction and visualization of cultural heritage: analyzing our legacy through time. *International Archives of Photogrammetry, Remote Sensing and Spatial Information Sciences*, 42(2/W3): 609–616.

Snavely, N., Seitz, S.M. and Szeliski, R., 2008. 'Modeling the world from Internet photo collections', *International Journal of Computer Vision*, 80(2), pp. 189-210.

"The Arches", 2024. Overview of the history of "The Arches" of Newcastle University. https://co-curate.ncl.ac.uk/the-arches-newcastle-university/, last accessed 04/11/2024.

Vindolanda, 2024. Roman Fort Vindolanda Charitable Trust. https://www.vindolanda.com/.

Vindolanda Tablets Online, 2024. Vindolanda database of writing tablets. http://vindolanda.csad.ox.ac.uk/.

Wan, Y., 2024. A comparison between low-cost and professional RTK equipment under forest conditions. Master's thesis in Master Programme Wireless, Photonics and Space Engineering, Chalmers University of Technology, Sweden.

Xiao, W., Mills, J., Guidi, G., Rodriguez-Gonzalvez, P., Gonizzi Barsanti, S., Gonzalez-Aguilera, D., 2018. Geoinformatics for the conservation and promotion of cultural heritage in support of the UN Sustainable Development Goals. *ISPRS Journal of Photogrammetry and Remote Sensing*, 142: 389–406.